## NANO LETTERS

2009 Vol. 9, No. 12 4268-4272

## **Evolution of Graphene Growth on Ni and Cu by Carbon Isotope Labeling**

Xuesong Li,† Weiwei Cai,† Luigi Colombo,\*,‡ and Rodney S. Ruoff\*,†

Department of Mechanical Engineering and the Texas Materials Institute, 1 University Station C2200, The University of Texas at Austin, Austin, Texas 78712-0292, and Texas Instruments Incorporated, Dallas, Texas 75243

Received August 3, 2009

## **ABSTRACT**

Large-area graphene growth is required for the development and production of electronic devices. Recently, chemical vapor deposition (CVD) of hydrocarbons has shown some promise in growing large-area graphene or few-layer graphene films on metal substrates such as Ni and Cu. It has been proposed that CVD growth of graphene on Ni occurs by a C segregation or precipitation process whereas graphene on Cu grows by a surface adsorption process. Here we used carbon isotope labeling in conjunction with Raman spectroscopic mapping to track carbon during the growth process. The data clearly show that at high temperatures sequentially introduced isotopic carbon diffuses into the Ni first, mixes, and then segregates and precipitates at the surface of Ni forming graphene and/or graphite with a uniform mixture of  $^{12}$ C and  $^{13}$ C as determined by the peak position of the Raman G-band peak. On the other hand, graphene growth on Cu is clearly by surface adsorption where the spatial distribution of  $^{12}$ C and  $^{13}$ C follows the precursor time sequence and the linear growth rate ranges from about 1 to as high as 6  $\mu$ m/min depending upon Cu grain orientation. This data is critical in guiding the graphene growth process as we try to achieve the highest quality graphene for electronic devices.

Graphene, a monolayer of sp<sup>2</sup>-bonded carbon atoms or one monolayer of graphite, has attracted interest in part because of its unique transport properties.1 The surface science community has published extensively on what is referred to as "monolayer graphite", that is, graphene, as grown on various metal films that are epitaxially well matched to graphene.2 To date, devices have been fabricated mostly on exfoliated graphene, 1 chemically reduced graphite oxide, 3-6 graphene formed by ultrahigh vacuum (UHV) annealing of single crystal SiC,<sup>7,8</sup> and that grown on metal substrates.<sup>9–15</sup> However, exfoliated graphene still shows superior transport properties compared to all other sources. Graphene obtained on SiC single crystals has good mobility, but this material may be limited to devices on SiC only, since transfer to other substrates such as SiO<sub>2</sub>/Si has not been demonstrated yet and might be difficult. There have been a number of reports on the growth of graphene on metal substrates such as Ni, Co, Ru, Ir, Cu, etc., by UHV-chemical vapor deposition (CVD)<sup>9-11</sup> or "normal" CVD.<sup>12-15</sup> Because of cost, grain size, etchability, and their wide use and acceptance by the semiconductor industry, Ni and Cu have received the most attention as a graphene substrate material. Several groups have already demonstrated the growth of graphene and fewlayer graphene (FLG) on polycrystalline Ni<sup>12-14</sup> while large

and the bond force constants are equal<sup>16</sup>

area graphene has been grown on Cu15 substrates by CVD.

It has been proposed that CVD growth of graphene on Ni is

due to a C segregation<sup>12</sup> or precipitation<sup>13</sup> process and that

a fast cooling rate in conjunction with thin films are needed

to suppress the formation of multiple graphene layers. 12,14

But to date the graphene films grown on Ni foils or on Ni

thin films have not yielded uniform graphene layers, that is,

they have a wide variation in thickness over the metal surface

from a monolayer to many layers. Recently, in a different

publication, we have shown that Cu is an excellent candidate

for making large-area graphene films with uniform thickness

due to the low solubility of C in Cu.<sup>15</sup> In that publication it was suggested that the graphene growth is somehow surface mediated and self-limiting.

In this work, we used isotopic labeling of the carbon precursor to study the mechanism and kinetics of CVD growth of graphene on Ni and Cu substrates. We took advantage of the separation of the <sup>12</sup>C and <sup>13</sup>C Raman modes to observe the spatial distribution of graphene domains. The frequencies of Raman modes are given by eq 1 with the assumption that the <sup>12</sup>C or <sup>13</sup>C atoms are randomly mixed

 $<sup>\</sup>omega = \omega_{12} \sqrt{\frac{m_{12}}{n_{12}m_{12} + n_{13}m_{13}}} \tag{1}$ 

<sup>\*</sup> To whom correspondence should be addressed. E-mail: (R.S.R.) r.ruoff@mail.utexas.edu; (L.C.) colombo@ti.com.

<sup>†</sup> The University of Texas at Austin.

<sup>\*</sup> Texas Instruments Incorporated.

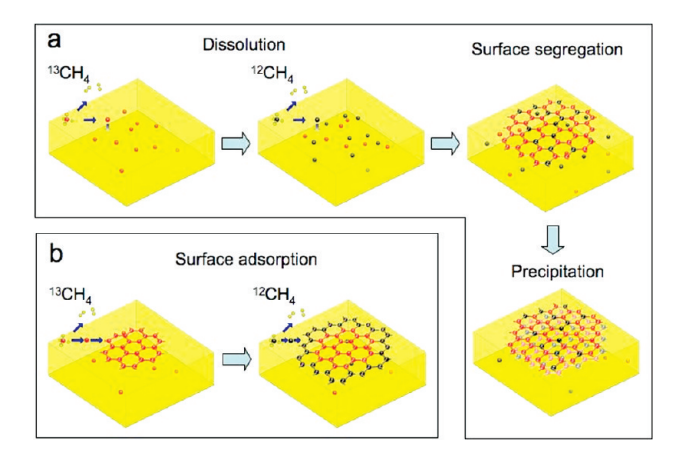


**Figure 1.** Schematic diagrams of the possible distribution of C isotopes in graphene films based on different growth mechanisms for sequential input of C isotopes. (a) Graphene with randomly mixed isotopes such as might occur from surface segregation and/or precipitation. (b) Graphene with separated isotopes such as might occur by surface adsorption.

where  $\omega_{12}$  is the Raman mode frequency of <sup>12</sup>C graphene/ graphite,  $n_{12}$  and  $n_{13}$  are the atomic fractions, and  $m_{12}$  and  $m_{13}$  are the atomic masses of <sup>12</sup>C and <sup>13</sup>C, respectively.

We used thin Ni film ( $\sim$ 700 nm, deposited by sputtering on SiO<sub>2</sub>/Si wafer) rather than on Ni foil to minimize the saturation time and the amount of carbon in the Ni film since the solubility of C in Ni is high, about  $\sim$ 0.9 at. % at 900 °C. For Cu, we used foils having a thickness of 25  $\mu$ m since the carbon solubility is negligible. The experimental procedure for graphene growth is similar to that reported previously 15 with a deposition temperature of 900 °C for Ni and 1000 °C for Cu. However, in this work both normal methane and  $^{13}$ CH<sub>4</sub> (99.95% pure) were introduced to the growth chamber in a specific sequence. The duration of exposure of methane is defined as  $^{j}t_{i}$  as, where j=12 or 13 denotes  $^{12}$ CH<sub>4</sub> or  $^{13}$ CH<sub>4</sub>, and i denotes the step in the sequence (e.g.,  $^{13}t_{1}$  means the first gas introduced was  $^{13}$ CH<sub>4</sub> with the duration of exposure being  $t_{1}$ ).

Figure 1 shows schematically the possible distributions of <sup>12</sup>C and <sup>13</sup>C in graphene films based on different assumed growth mechanisms when 12CH4 or 13CH4 are introduced sequentially. We want to emphasize that "segregation" and "precipitation" should be distinguished as different concepts, which have been well explained by Shelton et al., <sup>17</sup> that is, segregation refers to compositional heterogeneity in thermal equilibrium under conditions which correspond to a "onephase" field, while precipitation refers to inhomogeneities that arise as a result of equilibrium "phase separation". Blakely and coauthors have performed extensive studies on the formation of carbon films by cooling Ni foils saturated with C at high temperatures and found that a monolayer graphite grows first by C segregation, followed by more C precipitation thus forming graphite. 17-20 This previous work can be extended to explain CVD growth of FLG films on Ni film as well, as will be demonstrated in the following section. Figure 1a shows the case of carbon segregation from the bulk to the metal surface followed by precipitation growth. In the case of metals like Ni where the carbon

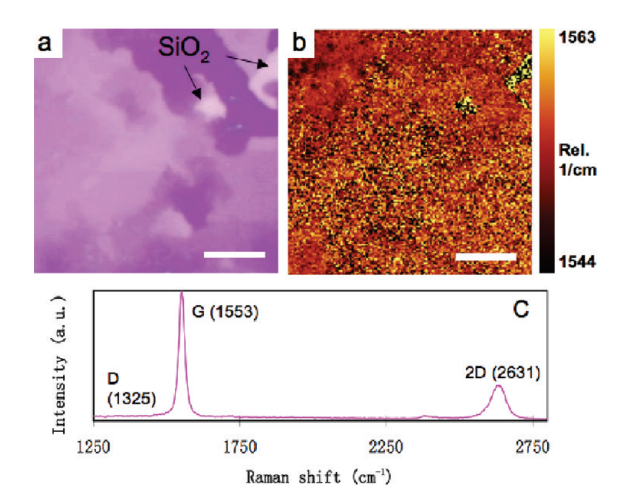


**Figure 2.** Optical micrograph and distribution of C isotopes in a FLG film grown on Ni. (a) An optical micrograph of a FLG film transferred onto a SiO<sub>2</sub>/Si wafer. (b) The corresponding Raman map of location of the G bands and (c) a typical Raman spectrum from this film, showing the film consists of randomly mixed isotopes (with an overall composition of  $\sim$ 45%  $^{13}$ C and  $\sim$ 55%  $^{12}$ C). Scale bars are 5  $\mu$ m.

solubility is high, carbon diffuses into the metal first before segregating and precipitating to the surface. As a result, sequential dosing of <sup>12</sup>CH<sub>4</sub> and <sup>13</sup>CH<sub>4</sub> is expected to yield a uniform C-metal solution, and the segregated and/or precipitated graphene will consist of randomly mixed isotopes (Figure 1a). In contrast, if carbon does not diffuse into the metal, graphene grown with the sequential dosing of <sup>12</sup>CH<sub>4</sub> and <sup>13</sup>CH<sub>4</sub> grows by surface adsorption and the isotope distribution in the local graphene regions will reflect the dosing sequence employed (Figure 1b).

Figure 2 shows the results of graphene growth on Ni film. We evaluated several sets of feeding time sequences of C isotopes on Ni films, but no distinguishable separation of isotopes was found. Figure 2a shows an optical micrograph of a graphene film grown on a Ni film  $(^{13}t_{1,3,5,7} = ^{12}t_{2,4,6,8} =$ 1 min) and transferred onto a SiO<sub>2</sub>/Si wafer by poly (methyl methacrylate) (PMMA) similar to the reported method. 15,21 The variation of color contrast indicates the film is not uniform in thickness and consists of one to tens of graphene layers. Figure 2b further shows the map of the G band and Figure 2c shows a typical Raman spectrum from this FLG film, which is located at  $\sim 1553$  cm<sup>-1</sup>, corresponding to the composition of 45%-13C/ 55%-12C according to eq 1. The uniformity of the G-band and the uniform shift according to eq 1 demonstrates the uniformity of the <sup>12</sup>C and <sup>13</sup>C distribution across the metal surface supporting the idea that the growth mechanism is as that described in Figure 1a.

Figure 3 shows the results of graphene grown on Cu foils  $(^{13}t_{1,3,5,7}=^{12}t_{2,4,6,8}=1 \text{ min})$ . Figure 3a shows an optical micrograph of the resulting graphene film transferred onto a SiO<sub>2</sub>/Si substrate using PMMA as the carrier material for transfer as previously reported. The surface of the transferred graphene is relatively uniform with the exception of wrinkles that are believed to be formed during cool-down. The wrinkles are a result of the different coefficient of thermal expansion between graphene/graphite and the underlying metal substrate.  $^{22,23}$ 

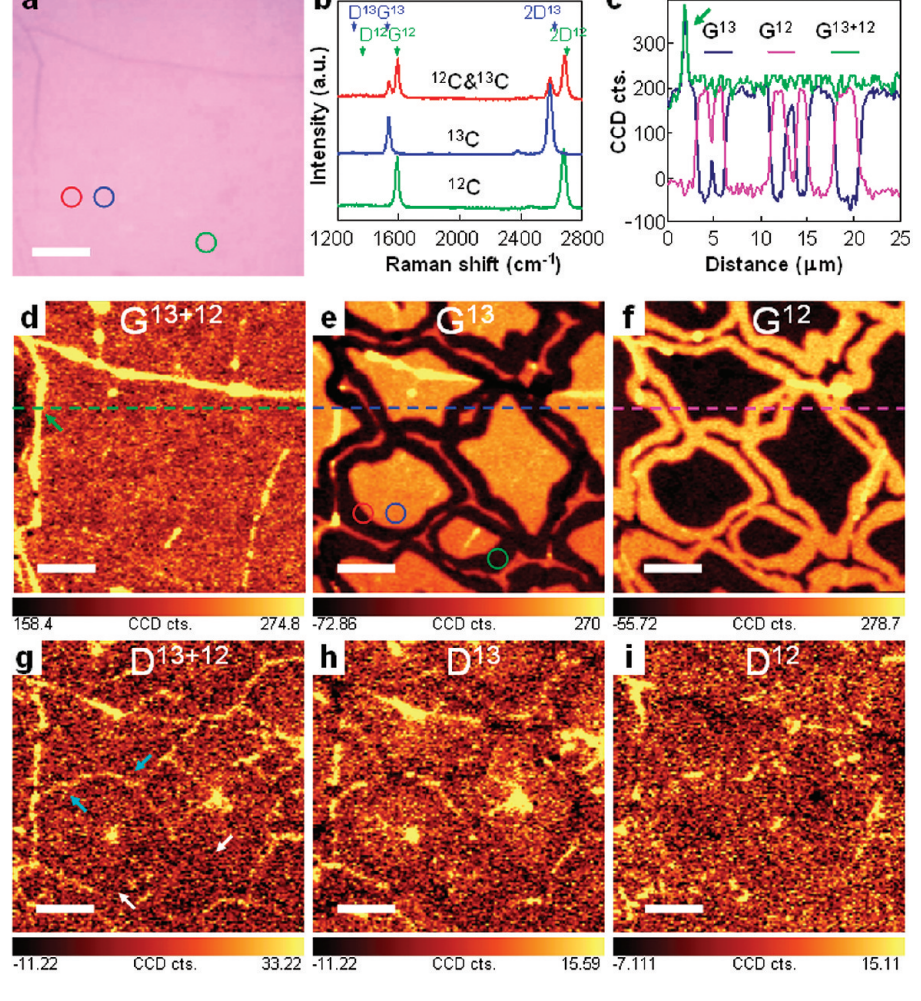


**Figure 3.** Micro-Raman characterization of the isotope-labeled graphene grown on Cu foil and transferred onto a SiO<sub>2</sub>/Si wafer. (a) An optical micrograph of the identical region analyzed with micro-Raman spectroscopy. (b) Raman spectra from  $^{12}$ C-graphene (green),  $^{13}$ C-graphene (blue), and the junction of  $^{12}$ C- and  $^{13}$ C-graphene (red), respectively, marked with the corresponded colored circles in (a) and (e). (c) Line scan of the dashed lines in (d-f). Integrated intensity Raman maps of (d)  $G^{13+12}(1500-1620 \text{ cm}^{-1})$ , (e)  $G^{13}(1500-1560 \text{ cm}^{-1})$ , (f)  $G^{12}(1560-1620 \text{ cm}^{-1})$ , (g)  $D^{13+12}(1275-1375 \text{ cm}^{-1})$ , (h)  $D^{13}(1275-1325 \text{ cm}^{-1})$ , and (i)  $D^{12}(1325-1375 \text{ cm}^{-1})$  of the area shown in (a). Scale bars are 5  $\mu$ m.

The Raman spectra, Figure 3b, show the presence of graphene with regions having close to pure <sup>12</sup>C from natural methane (~99% <sup>12</sup>CH<sub>4</sub>), regions of isotopically pure <sup>13</sup>C, and regions where both <sup>12</sup>C and <sup>13</sup>C are present. An analysis of both the color contrast of the optical micrograph, <sup>24</sup> and the Raman spectra <sup>13,25-27</sup> show that the carbon layer is a monolayer of graphite, that is, graphene. When the Raman laser beam was focused at the junction of <sup>12</sup>C and <sup>13</sup>C graphene regions, the characteristic bands for both <sup>12</sup>C and <sup>13</sup>C graphene appeared in the spectrum. The intensity of each band depends on the area occupied by each isotopically labeled region under the laser spot and the sum of the intensity of two bands (e.g., G<sup>13</sup> + G<sup>12</sup>) was found to be essentially equal to that of the intensity from either the pure <sup>13</sup>C or <sup>12</sup>C regions of the graphene film.

Figures 3d-i shows the Raman G and D band maps of the graphene film shown in Figure 3a for both <sup>12</sup>C and <sup>13</sup>C. Figure 3d is a map of the overall G band intensity (G<sup>13</sup> + G<sup>12</sup>) of the area shown in Figure 3a. The uniform intensity distribution demonstrates that the thickness is uniform except for the wrinkles (bright lines). Figure 3e,f shows the maps

of the G-band of <sup>13</sup>C and of <sup>12</sup>C, respectively, which show the time evolution of graphene growth. The bright solid centers in the G13 map in Figure 3e correspond to 13Cgraphene grown during  $^{13}t_1$ ; the low intensity, dark rings correspond to  ${}^{12}\text{C-graphene}$  grown during  ${}^{12}t_2$ , which are seen as bright rings in the G12 map in Figure 2f; the bright area between the dark rings in Figure 3e corresponds to <sup>13</sup>Cgraphene grown during  $^{13}t_3$ . Figure 3c shows a line scan (marked with dashed lines across Figures 2d-f) where the <sup>12</sup>C-graphene and <sup>13</sup>C-graphene domains are clearly seen with the blue line representing the G<sup>13</sup> (i.e., <sup>13</sup>C-graphene) domains and the pink line representing the G<sup>12</sup> (i.e., <sup>12</sup>C-graphene) domains. The green line, which is the most uniform across the film, is the overall G band intensity  $(G^{13} + G^{12})$  with the peak corresponding to the wrinkle in the film. It is interesting to note that we flowed eight cycles of alternating <sup>12</sup>CH<sub>4</sub> and <sup>13</sup>CH<sub>4</sub> but the resulting graphene grew only during the first three dosings. The fourth and subsequent doses played no role because the surface was already saturated with graphene. These data show that single layer graphene on Cu grows in less than 3 min under the conditions we used,

growth occurs in two-dimensions and thus is a consequence of a surface-adsorption process, and that growth is selflimiting since there is no catalyst to promote decomposition and growth after the first layer of carbon (graphene) is deposited.

The films grown on Cu show a nonuniform presence of the Raman D-band. The D maps in Figure 3g-i provide additional information. Other than the high intensity of the D band from the wrinkles, some bright spots and lines are also seen corresponding to defective centers and boundaries between graphene domains, respectively. We define a domain as the area of graphene grown from one nucleus. The domain size will depend on the specific growth conditions and for the conditions used in this work the diameter of the domain is about 10  $\mu$ m. The interdomain defects can occur where the graphene domains join, for example in the current case, after  $^{13}t_3$ , defects are observed as indicated by the blue arrows in Figure 3g. The nature of the defects could be the formation of pentagonal and/or heptagonal arrangements of carbon atoms that form mis-oriented graphene domains resulting from the Cu surface roughness, as was found for Ir.<sup>28</sup> In contrast, the low defect boundaries (indicated by the white arrows in Figure 3g) may indicate a "good" registration between two domains. A detailed understanding of such defects is suggested for future work. Careful observation of the optical micrograph (Figure 3a) and the Raman maps (Figures 3d-i) shows that there is no overlap of the graphene layers where the domains join, suggesting that there is crystallographic registration to the Cu substrate. If there were overlap, a high contrast or bright line would be present in the micrograph and the G-band Raman maps. This sequential distribution of <sup>13</sup>C and <sup>12</sup>C clearly shows that graphene growth on Cu is based on the surface adsorption mechanism.

As we reported previously,<sup>15</sup> there can also be a small fraction of few-layer flakes stacked on the graphene film. For the samples discussed here, Raman imaging showed that these flakes also consist of separated <sup>13</sup>C and <sup>12</sup>C rings, indicating that they grow by surface adsorption, but not by segregation/ precipitation (Figure 4). These flakes show the same or smaller number of isotopic sequential rings as the first layer graphene, indicating that flake growth stops once the Cu surface is fully covered with graphene. Termination of flake growth due to the full coverage of Cu surface with graphene suggests that the carbon source for flake growth is from the catalytic decomposition of methane by the active Cu surface. Further work is necessary to understand the exact origin of the flake defects.

We also studied the graphene growth rate from the growing front of either  $^{12}\text{CH}_4$  or  $^{13}\text{CH}_4$ . For the case of the first graphene layer, the edge growth rate for the first minute is  $3-6~\mu\text{m}/\text{min}$  and for the second minute it is  $1-2~\mu\text{m}/\text{min}$ . The growth rate is found to be dependent on the Cu grain orientation as was previously observed by scanning electron microscopy imaging of an interrupted growth runs.  $^{15}$  The domain advancement rate that decrease with time could be associated with a decrease in the number of catalytic sites as the domains fill the Cu surface area. This will require further investigation and the subject of a future publication. In contrast, the growth rate of the second

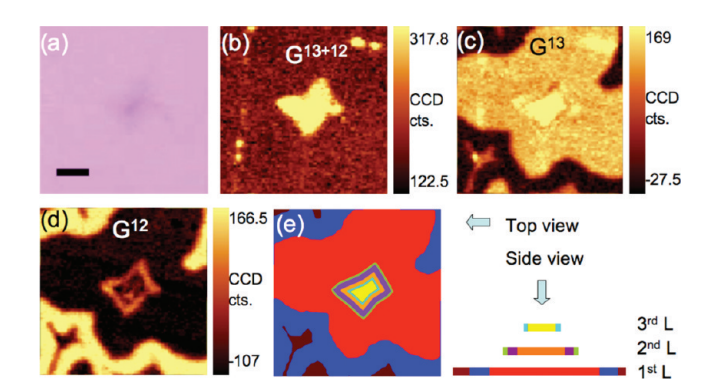


**Figure 4.** Raman imaging spectroscopy of few-layer (FL) regions. (a) Optical micrograph. (b-d) Raman maps of overall G,  $G^{13}$ , and  $G^{12}$ , respectively, corresponding to the region in (a). The FL regions can be easily located from the optical micrograph due to their high contrast (a) and also from their high intensity in the overall G map (b). The layer and growth sequences are schematically shown in (e), where red, orange, yellow show  $^{13}$ C grown in the first minute, blue, purple, teal show  $^{12}$ C grown in the second minute, and maroon, lime show  $^{13}$ C grown in the third minute. Scale bar is 2  $\mu$ m.

and third layers is slower (<160 and <40 nm/min, respectively), and the multilayer flakes thus occupy a very small area (<5%) of the whole film. The slower growth rate of higher order layers may be attributed to a much lower concentration of Cu catalyst available to promote the decomposition of methane in these regions.

The two mechanisms of graphene growth on Ni and Cu can be understood from the C-metal binary phase diagram. The binary phase diagrams of C-Ni and C-Cu are similar in that C has a limited solubility in the metal without the presence of a metal-carbide line compound. The only significant difference is that the solubility of C in Cu is much lower than that in Ni. Since only a small amount of carbon can be dissolved in Cu, the source for graphene formation is mainly from the CH<sub>4</sub> that is catalytically decomposed on the Cu surface with minimal carbon diffusion into the Cu. As mentioned previously, once the surface is fully covered with graphene growth terminates because of the absence of a catalyst to decompose CH<sub>4</sub>. In contrast, Ni can dissolve more carbon atoms and hence it is difficult to get uniform graphene films due to precipitation of extra C during the cool-down. The C precipitation process is a nonequilibrium process, which should be suppressed if one aims to achieve monolayer graphene growth, for example, by using a controlled thin Ni film and/or high cooling rate. 12-14 However, because of microstructural defects, predominantly grain boundaries, it is very difficult to fully eliminate the effect of precipitation for metals with high carbon solubility. Hence, metals with low C solubility such as Cu offer a possible path to large-area growth of graphene. Discrete regions of isotopically labeled graphene such as presented here for growth on Cu may also yield novel devices and transport physics in future studies.

**Acknowledgment.** We would like to thank the Nanoelectronic Research Initiative (NRI-SWAN; no. 2006-NE-1464), the DARPA CERA Center, and The University of Texas at Austin for support.

## References

- (1) Geim, A. K.; Novoselov, K. S. Nat. Mater. 2007, 6 (3), 183-191.
- (2) Greber, T. [Online early access.] DOI: arXiv:0904.1520v1, 2009.
- (3) Dikin, D. A.; Stankovich, S.; Zimney, E. J.; Piner, R. D.; Dommett, G. H. B.; Evmenenko, G.; Nguyen, S. T.; Ruoff, R. S. *Nature* 2007, 448 (7152), 457–460.
- (4) Gilje, S.; Han, S.; Wang, M.; Wang, K. L.; Kaner, R. B. Nano Lett. 2007, 7 (11), 3394–3398.
- (5) Stankovich, S.; Dikin, D. A.; Dommett, G. H. B.; Kohlhaas, K. M.; Zimney, E. J.; Stach, E. A.; Piner, R. D.; Nguyen, S. T.; Ruoff, R. S. *Nature* 2006, 442 (7100), 282–286.
- (6) Park, S.; Ruoff, R. S. Nat. Nanotechnol 2009, 4, 217-224.
- (7) Berger, C.; Song, Z.; Li, X.; Wu, X.; Brown, N.; Naud, C.; Mayou, D.; Li, T.; Hass, J.; Marchenkov, a. A. N.; Conrad, E. H.; First, P. N.; de Heer, W. A. *Science* 2006, 312, 1991–1996.
- (8) Emtsev, K. V.; Bostwick, A.; Horn, K.; Jobst, J.; Kellogg, G. L.; Ley, L.; McChesney, J. L.; Ohta, T.; Reshanov, S. A.; Rohrl, J.; Rotenberg, E.; Schmid, A. K.; Waldmann, D.; Weber, H. B.; Seyller, T. Nat. Mater. 2009, 8 (3), 203–207.
- (9) Marchini, S.; Gunther, S.; Wintterlin, J. Phys. Rev. B 2007, 76 (7), 075429.
- (10) Loginova, E.; Bartelt, N. C.; Feibelman, P. J.; McCarty, K. F. New J. Phys. 2008, 10, 093026.
- (11) Sutter, P. W.; Flege, J.-I.; Sutter, E. A. Nat. Mater. 2008, 7, 406–411.
- (12) Yu, Q.; Lian, J.; Siriponglert, S.; Li, H.; Chen, Y. P.; Pei, S.-S. Appl. Phys. Lett. 2008, 93, 113103.
- (13) Reina, A.; Jia, X.; Ho, J.; Nezich, D.; Son, H.; Bulovic, V.; Dresselhaus, M. S.; Kong, J. Nano Lett. 2009, 9, 30–35.
- (14) Kim, K. S.; Zhao, Y.; Jang, H.; Lee, S. Y.; Kim, J. M.; Kim, K. S.; Ahn, J.-H.; Kim, P.; Choi, J.-Y.; Hong, B. H. *Nature* 2009, 457, 706–710

- (15) Li, X. S.; Cai, W. W.; An, J. H.; Kim, S.; Nah, J.; Yang, D. X.; Piner, R. D.; Velamakanni, A.; Jung, I.; Tutuc, E.; Banerjee, S. K.; Colombo, L.; Ruoff, R. S. Science 2009, 324, 1312.
- (16) Fan, S.; Liu, L.; Liu, M. Nanetechnology 2003, 14, 1118-1123.
- (17) Shelton, J. C.; Patil, H. R.; Blakely, J. M. Surf. Sci. **1974**, 43, 493–520
- (18) Isett, L. C.; Blakely, J. M. Surf. Sci. 1976, 58 (2), 397-414.
- (19) Eizenberg, M.; Blakely, J. M. Surf. Sci. 1979, 82 (1), 228-236.
- (20) Eizenberg, M.; Blakely, J. M. J. Chem. Phys. **1979**, 71 (8), 3467–3477.
- (21) Reina, A.; Son, H.; Jiao, L.; Fan, B.; Dresselhaus, M. S.; Liu, Z. F.; Kong, J. J. Phys. Chem. C 2008, 112, 17741–17744.
- (22) Cai, W. W.; Piner, R. D.; Stadermann, F. J.; Park, S.; Shaibat, M. A.; Ishii, Y.; Yang, D. X.; Velamakanni, A.; An, S. J.; Stoller, M.; An, J. H.; Chen, D. M.; Ruoff, R. S. Science 2008, 321 (5897), 1815– 1817.
- (23) Obraztsov, A. N.; Obraztsova, E. A.; Tyurnina, A. V.; Zolotukhin, A. A. Carbon 2007, 45, 2017–2021.
- (24) Ni, Z. H.; Wang, H. M.; Kasim, J.; Fan, H. M.; Yu, T.; Wu, Y. H.; Feng, Y. P.; Shen, Z. X. *Nano Lett.* **2007**, *7* (9), 2758–2763.
- (25) Ferrari, A. C.; Meyer, J. C.; Scardaci, V.; Casiraghi, C.; Lazzeri, M.; Mauri, F.; Piscanec, S.; Jiang, D.; Novoselov, K. S.; Roth, S.; Geim, A. K. Phys. Rev. Lett. 2006, 97, 187401.
- (26) Casiraghi, C.; Pisana, S.; Novoselov, K. S.; Geim, A. K.; Ferrari, A. C. Appl. Phys. Lett. 2007, 91, 233108.
- (27) Das, A.; Pisana, S.; Chakraborty, B.; Piscanec, S.; Saha, S. K.; Waghmare, U. V.; Novoselov, K. S.; Krishnamurthy, H. R.; Geim, A. K.; Ferrari, A. C.; Sood, A. K. Nat. Nanotechnol. 2008, 3, 210– 215.
- (28) Coraux, J.; N'Diaye, A. T.; Busse, C.; Michely, T. Nano Lett. 2008, 8 (2), 565–570.

NL902515K